Study of charge transport properties in a ZnO/CdS/Cu(In,Ga)Se_2 solar cell via admittance spectroscopy

Sanjoy Paul[a] and Roberto Lopez
Department of Physics, and Material Science, Engineering, and Commercialization Program Texas State University, San Marcos, Texas 78666

Ingrid L. Repins
National Renewable Energy Laboratory (NREL), Golden, Colorado 80401

Jian V. Li[b]
Department of Aeronautics and Astronautics, National Cheng Kung University, Tainan 70101, Taiwan and Department of Physics, and Material Science, Engineering, and Commercialization Program Texas State University, San Marcos, Texas 78666

(Received 9 November 2017; accepted 22 January 2018; published 13 February 2018)

The authors investigate the charge carrier transport properties in a thin-film heterojunction Cu(In,Ga)Se_2 (CIGS) solar cell device via coordinated capacitance–voltage and admittance spectroscopic measurements. The CIGS absorber width was measured using temperature dependent depletion width in the freeze-out regime and its acceptor density extracted from conventional capacitance–voltage analysis in the non-freeze-out regime. The bias-dependent modified dielectric relaxation in the Cu(In,Ga)Se_2 solar cell was exploited to extract the absorber's resistivity, hole mobility, and their temperature dependency, all by admittance spectroscopy. In the temperature range of 133–300 K, the extracted hole mobility in the CIGS device increases from 7.55×10^{-3} to 4.08 $cm^2/V\,s$ with temperature. The temperature dependent resistivity and mobility show Arrhenius behavior with an activation energy ≈120 meV. The thermally activated behavior of mobility is related to the potential fluctuation encountered by the holes during their transport, which enables admittance spectroscopy to directly measure the potential fluctuation in the CIGS polycrystalline material. *Published by the AVS.* https://doi.org/10.1116/1.5013046

I. INTRODUCTION

Thin-film based Cu(In,Ga)Se_2 (CIGS) solar cells are promising photovoltaic (PV) devices and have attracted worldwide attention for solar energy conversion with champion devices exhibiting efficiency of 22.6%.[1] The CIGS absorber material is of direct bandgap tunable with Ga content, possesses high absorption coefficient, and allows optimized match to the solar spectrum and hence high efficiency.[2,3] In developing high-quality CIGS materials and high-performance devices, understanding the critical parameters such as charge carrier density, resistivity/conductivity, mobility, and their temperature dependency is important both from scientific and technological perspectives. In particular, carrier mobility in the CIGS materials is a key parameter to both contact resistance and carrier collection efficiency yet less understood than that in the single-crystal PV materials such as Si.

There are several characterization methods of which Hall and pulsed laser time-of-flight are most popular to extract the charge carrier mobility and study transport phenomena in semiconductors. The Hall mobility measurement technique is well established, but it applies only to the absorber level (i.e., in the early stage of device fabrication)[4–7] and requires the exclusion of conductive sublayers such as molybdenum. The pulsed-laser time-of-flight drift mobility measurement is particularly suitable for materials possessing high resistivity and low carrier motility hence applied successfully to a range of insulating solids to liquids.[8–11] Due to the short duration of the laser pulse and its penetration depth, the time-of-flight technique requires thick films in order to have well defined flight distance.[12–14] Also, the built-in electric field in the solar cell device makes it complicated to use time-of-flight photo-transient method and requires specially designed time-of-flight technique and analysis method.[15] Admittance spectroscopy (AS), on the other hand, is an effective and proven method in extracting carrier concentration, resistivity, and mobility.[14,16–22] The biggest advantage of the admittance spectroscopic technique is that it can be applied to finished solar cells.[23,24]

The mobility in CIGS solar cells has been investigated using both admittance measurement and time-of-flight method.[21,25] However, there are few reports on the temperature dependency of hole mobility and resistivity. This study demonstrates the use of coordinated capacitance-voltage and simplified admittance spectroscopy techniques to estimate the resistivity and mobility, and their dependency on temperature with a lightly doped Cu(In,Ga)Se_2 solar cell. The temperature dependence of mobility may reveal the dominant mechanism governing carrier scattering and transport. In our specific case of CIGS thin-film materials, the mechanism of interest here is potential fluctuation, which is to be measured from the thermal behavior of mobility.

II. METHOD

The AS, because its realization only requires accessing the electrical AC response of the device via electrodes, is a

[a]Electronic mail: sanjoy.paul@txstate.edu
[b]Electronic mail: jianvli@mail.ncku.edu.tw

convenient electrical characterization technique to study the complete solar cell. This involves the measurement of admittance (Y), i.e., the capacitance (C) and conductance (G) in a rectifying junction as a function of angular frequency ω ($\omega = 2\pi f$, $f =$ linear frequency) and temperature (T). In this technique, the complex admittance is defined as $Y(\omega, T) = G(\omega, T) + j\omega C(\omega, T)$, where $j^2 = -1$.

The energy band diagram for a generic ZnO/n-CdS/p-CIGS heterostructures is shown in Fig. 1(a) to depict the depletion and quasineutral regions. The equivalent circuit of the CIGS absorber, as shown in Fig. 1(a) inset, can be modeled as the series connection of the depletion capacitance (C_d) and a circuit unit consisting of the parallel connection of bulk conductance (G_g') and capacitance (C_g') in the quasineutral region.[24]

The response of the majority carrier particularly at a frequency (ω) of the AC signal is limited by the dielectric relaxation time τ_{dr} ($\tau_{dr} = 2\pi/\omega_{dr}$; $\omega_{dr} = 1/\rho\varepsilon$), where, ρ is the resistivity of the material and ε is the dielectric permittivity. For frequency $\omega < \omega_{dr}$, the absorber in the quasineutral region behaves as a conductor with bulk conductance $G_g' = A/\rho(t - W)$, where A is the cell area, W the depletion width, and t the absorber thickness. Whereas, for $\omega > \omega_{dr}$, the quasineutral absorber behaves like a capacitor with bulk capacitance $C_g' = \varepsilon A/(t - W)$. The admittance analysis of the equivalent circuit of CIGS using a small AC signal leads to the following equation:[21]

$$C = C_d \frac{1 + (C_d/C_g)(\rho\varepsilon\omega)^2}{1 + (C_d/C_g)^2(\rho\varepsilon\omega)^2},$$
$$\frac{G}{\omega} = C_d \frac{(C_d/C_g - 1)(\rho\varepsilon\omega)}{1 + (C_d/C_g)^2(\rho\varepsilon\omega)^2}. \quad (1)$$

Experimentally, the capacitance versus frequency plot, as shown in Fig. 1(b) shows step transition with an inflection frequency (ω_p) below which C approaches C_d and above which C approaches C_g, which is the series connection of C_d and C_g'. Using simple calculus and algebra, ω_p can be estimated via minimizing [see $\omega(dC/d\omega)$ vs ω plot in Fig. 1(b)] the expression in Eq. (1) and its expression is

$$\omega_p = \frac{W}{t}\left(\frac{1}{\rho\varepsilon}\right). \quad (2)$$

Because of the dependency of depletion width (W) with applied DC bias (V), $W \approx \sqrt{(2\varepsilon(V_{bi} - V)/qN_a)}$, ω_p depends on V. Where, N_a is the acceptor density, q is electronic charge, and V_{bi} is the built-in potential. The bias dependent inflection frequency (ω_p) in n^+-p junction is given by the relation

$$\omega_p{}^2 = \frac{W^2}{t^2}\left(\frac{1}{\rho\varepsilon}\right)^2 = \frac{2}{q\varepsilon N_a \rho^2 t^2}(V_{bi} - V). \quad (3)$$

Now, using Eq. (3) and from experimental data (ω_p^2 vs V plot), the slope can be used to extract the resistivity (ρ) and hence the mobility (μ) as

$$\rho = \sqrt{\frac{2}{q\varepsilon N_a t^2 \times \text{Slope}}} \quad (4)$$

and

$$\mu = \frac{1}{qN_a\rho} = \sqrt{\frac{\varepsilon t^2 \times \text{Slope}}{2qN_a}}. \quad (5)$$

In extracting ρ and μ, one uses the carrier concentration (N_a) determined from the capacitance-voltage (CV) measurement. Note that similar analysis can be performed using the conductance data instead of capacitance.

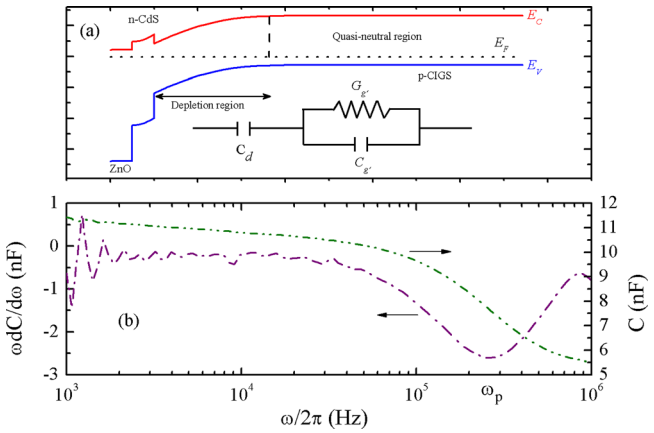

FIG. 1. (Color online) (a) Energy band diagram of a typical thin-film ZnO/n-CdS/p-CIGS solar cell and its equivalent circuit (inset). The depletion region is modeled as a depletion capacitance C_d. The quasineutral region is modeled as the parallel connection of geometrical capacitance (C_g') and the conductance (G_g'). (b) The frequency (ω) dependent capacitance (C) and differential capacitance ($\omega dC/d\omega$) spectra used to extract the inflection frequency (ω_p).

III. EXPERIMENT

The thin-film CIGS solar cell was fabricated in National Renewable Energy Laboratory. The cell structure is as follows: soda-lime glass substrate, sputtering deposited Mo back contact, p-CIGS deposited via coevaporation method by utilizing the standard three-stage recipe (Note, the substrate temperature of the growth was 435 °C), chemical-bath deposited n-CdS, sputtered ZnO, and e-beam evaporated Ni/Al grids for front-contact.

To perform the capacitance–voltage measurement and the admittance spectroscopy under dark condition, an Agilent 4294 impedance analyzer was used to collect the data. In CV measurement, the DC bias voltage was varied from −1.5 to 0.6 V while keeping an AC modulation amplitude of 50 mV (peak-to-peak) at 10 kHz frequency. For admittance spectroscopy, the DC bias and frequency were varied from −1.5 to 0.6 V and 10^2–10^8 Hz, respectively. The temperature dependent measurement was done using a He-cooled cryostat and temperature of the sample varied from 14 to 350 K with a step size of 7 K.

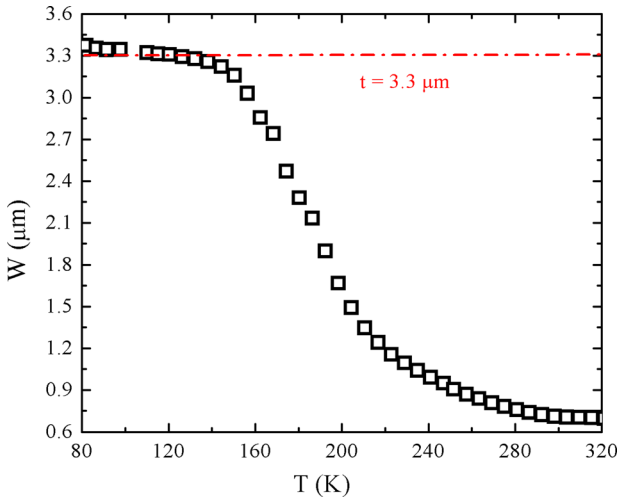

FIG. 2. (Color online) Variation of depletion width (W) at zero bias with temperature (T) to measure the absorber thickness. At lower temperatures (<150 K), the entire CIGS absorber becomes depleted and the thickness of the absorber is determined to be 3.3 μm using a dielectric constant value of 13.6.

IV. RESULTS AND DISCUSSION

Using the standard procedure related to abrupt one-sided n^+-p (n^+-CdS/p-CIGS) junction, we calculated the acceptor density (N_a) from the local derivative of Mott-Schottky ($1/C^2$ vs V) plot. For example (data not shown), we estimated the value of $N_a = 1.1 \times 10^{14}\,\mathrm{cm}^{-3}$ at T = 154 K. The dielectric constant of the CIGS absorber used in this calculation is 13.6. Following the temperature dependent CV analysis, we consider the temperature dependent depletion width (W) as shown in Fig. 2. At lower temperatures, the entire CIGS absorber becomes depleted and the thickness of the CIGS absorber (t) was estimated to be 3.3 μm in the complete carrier freeze-out region (<150 K), consistent with knowledge gained from CIGS film growth. In the following analysis, this thickness will be used in extracting the resistivity and mobility.

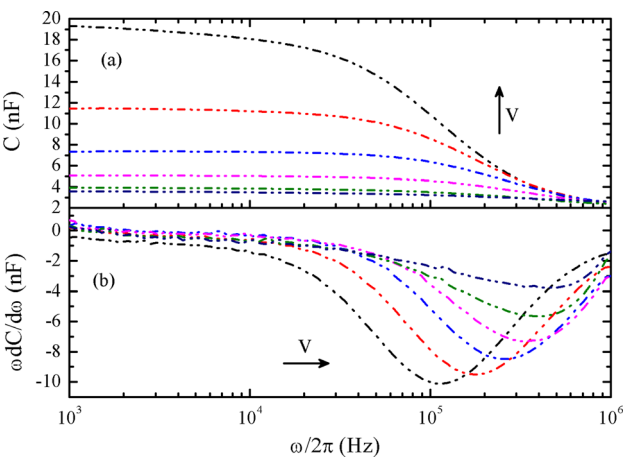

FIG. 3. (Color online) Bias (V) dependence of capacitance and differential capacitance spectra plotted against frequency of the CIGS solar cell at $T = 203$ K. The voltage change is from −0.4 to 0.1 V with voltage step $\Delta V = 0.1$ V.

The frequency dependent capacitance (C) and differential capacitance [$\omega(dC/d\omega)$] spectra of CIGS solar cell with different applied bias V (−0.4–0.1 V, $\Delta V = 0.1$ V) are shown in Fig. 3. The temperature in this case is 203 K. We present this for an example while similar behavior was observed at various other temperatures. In all cases, the depletion capacitance shows a step [Fig. 3(a)] at inflection frequency (ω_p) which was determined from the peak seen in the differential capacitance spectrum [Fig. 3(b)]. The transition frequency, ω_p, shifted toward higher frequency with bias is key to extracting the resistivity and carrier mobility.

The inflection frequencies (ω_p's) from the $\omega(dC/d\omega)$ vs $\omega/2\pi$ plot [as shown in Fig. 3(b)] were used to extract the resistivity (ρ) and mobility (μ) of CIGS. As expected from Eq. (3), the square of inflection frequency, ω_p^2, depends linearly on bias (V) as shown in Fig. 4(a). The measurement temperature for this data set was at 203 K. The linear fitting leads to $\rho = 1.86 \times 10^4\ \Omega\,\mathrm{cm}$ and $\mu = 0.19\,\mathrm{cm}^2/\mathrm{V\,s}$ using Eqs. (4) and (5). The acceptor density (extracted from CV measurement) at 203 K was $1.76 \times 10^{14}\,\mathrm{cm}^{-3}$.

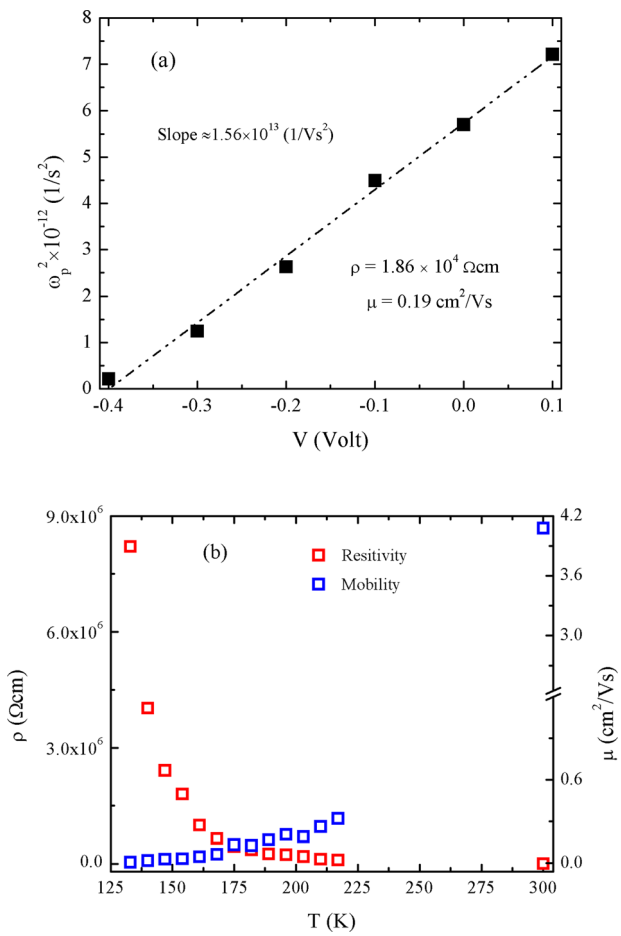

FIG. 4. (Color online) (a) Square of $\omega_p{}^2$ exhibit a linear dependence on the bias voltage (V) at $T = 203$ K as described in Eq. (3), from which a slope ($1.56 \times 10^{13}\,\mathrm{V}^{-1}\,\mathrm{s}^{-2}$) is determined. This leads to extraction of resistivity ($\rho = 1.86 \times 10^4\ \Omega\,\mathrm{cm}$) and hole mobility ($\mu = 0.19\,\mathrm{cm}^2/\mathrm{V\,s}$), respectively. (b) The temperature dependent (in the temperature range of 133–300 K) resistivity and mobility plots (on linear scale) extracted from admittance spectroscopic analysis.

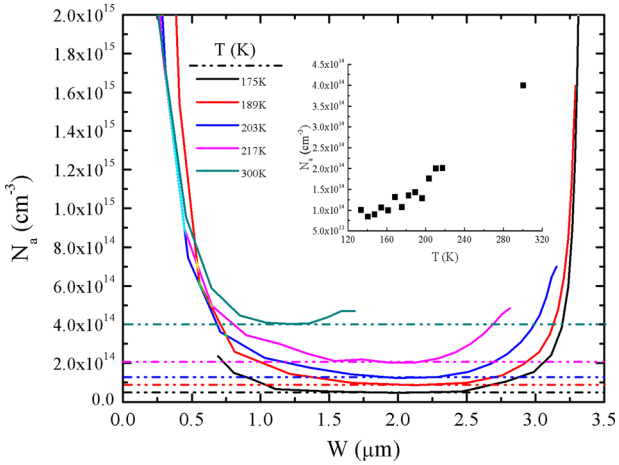

FIG. 5. (Color online) Temperature dependent acceptor density (N_a) profiles against the depletion width from which N_a is extracted from the flat region marked by broken horizontal lines. The inset shows the dependence of N_a with temperature (T) on a linear scale.

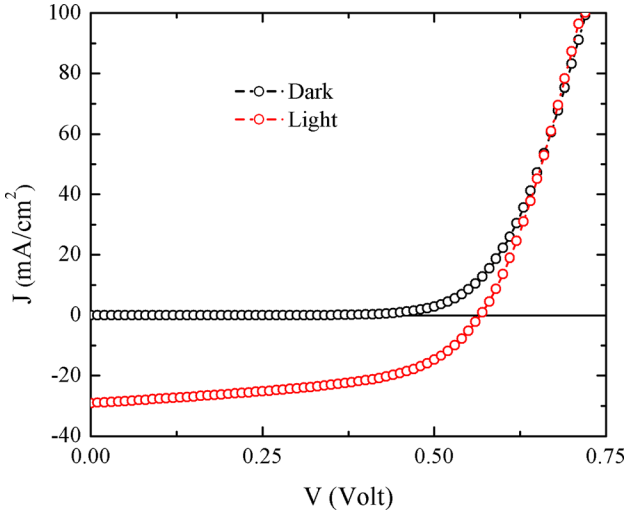

FIG. 6. (Color online) Dark and light current density–voltage characteristics of CIGS the CIGS solar cell. The intensity used is one sun. The cell parameters are: $V_{OC} = 0.566$ V, $J_{SC} = 29.12$ mA/cm^2, FF = 52.91%, and $\eta = 8.728\%$.

Figure 4(b) shows the temperature dependent resistivity and mobility in CIGS solar cells in the temperature 133 to 300 K. Exponential increase/decrease of mobility/resistivity are observed with increasing temperature. In the measured temperature range, the resistivity varies from 8.21×10^6 to 3.83×10^3 Ω cm and the mobility from 7.55×10^{-3} to 4.08 cm^2/V s, respectively.

Note that, in extracting the temperature dependent resistivity and mobility data, the temperature dependent carrier concentration was included. Figure 5 shows the depth profile of the apparent acceptor density (N_a) determined by the capacitance–voltage technique at various temperatures. The carrier concentration was chosen from the flat region (as indicated by broken horizontal lines). It was found that the carrier concentration depends weakly on temperature (varies between 1×10^{14}–4×10^{14} cm^{-3} over ~200 K as shown in the inset of Fig. 5) and exhibits a negligibly small activation energy <30 meV. This activation energy likely corresponds to the main acceptor level (copper vacancy) responsible for the p-type doping in the CIGS absorber. Traps may induce errors in the CV-extracted apparent carrier density, which is possible to correct using drive-level capacitance profiling (DLCP, not carried out in this work). Replacing CV-extracted carrier density with that more accurately extracted by DLCP may improve the mobility extraction according to the inverse square root dependency in Eq. (5). Note that, in the CIGS device investigated in this manuscript, no signature of trap other than the freezeout of majority carriers was observed in the frequency-temperature window (f: 10^2—10^8 Hz; T: 14–350 K) scanned.

Note that our acceptor density (for example, 4×10^{14} cm^{-3} at room temperature) is lower than high-efficiency device ($N_a \sim 10^{16}$ cm^{-3}). The low doping results in a poor device performance, i.e., low V_{OC}. Figure 6 show the dark and light (1 sun) current density-voltage (JV) characteristics of the solar cell used in this study. The cell parameters are: $V_{OC} = 0.566$ V, $J_{SC} = 29.12$ mA/cm^2, FF = 52.91%, and $\eta = 8.728\%$. The $V_{OC} = 0.566$ V is consistent with our acceptor density.

Our extracted hole mobility is lower than that measured by Lee *et al.* via high frequency admittance measurement in polycrystalline Cu(In,Ga)Se$_2$.[21] With various Cu(In,Ga)Se$_2$ cells with Ga content in the range of 0%–34%, the hole mobility μ_h in that report varies from 2.9 ± 0.3 to 22 ± 4.2 cm^2/V s. The reported temperature in their measurement is 150 K. Temperature independent hole mobility was reported by this group. Extracted mobility in our measurement at this temperature is $\approx 3.24 \times 10^{-2}$ cm^2/V s. On the other hand, our extracted hole mobility (4.08 cm^2/V s) at 300 K is larger than the reported value (0.6 cm^2/V s) by Dinca *et al.*[26] The method used in their measurement was a specially arranged pulsed laser time-of-flight technique. When extracting mobility via time-of-flight phototransient measurement, it is challenging to estimate the transit time of photogenerated charge carriers, which is the major factor in estimating the mobility at particular film thickness and electric field. Trapping and multiple trapping phenomena during the charge carrier's journey influenced the transient signal and hence the hole mobility. It is noteworthy that, the drift mobilities ranged from 0.02 to 0.7 cm^2/V s at room temperature with several CIGS cells fabricated different laboratories.[27] The presence of trap signature was observed in estimating electron mobility (0.02–0.05 cm^2/V s). Dinca *et al.* also reported weakly temperature dependent hole mobility (measured using time-of-flight method) in polycrystalline $CuIn_{1-x}Ga_xSe_2$ in the temperature range of 100–300 K.[27] Our experimental observation shows strong temperature dependency [as shown in Fig. 4(b)] in resistivity and hole mobility.

The temperature dependent resistivity or mobility are Arrhenius type (as shown in Fig. 7), i.e., thermally activated, and follows the Arrhenius equation ($\mu = \mu_0 e^{-E_{a,\mu}/k_B T}$ and $\rho = \rho_0 e^{E_{a,\rho}/k_B T}$, where are μ_0 and ρ_0 are mobility and resistivity prefactor, k_B is the Boltzmann's constant, $E_{a,\mu}$ is the activation energy of mobility, $E_{a,\rho}$ is the activation energy of resistivity, and T is the absolute temperature). Fitting the mobility and resistivity data with Arrhenius equation leads to the activation energies $E_{a,\mu} = 116 \pm 6$ meV (from

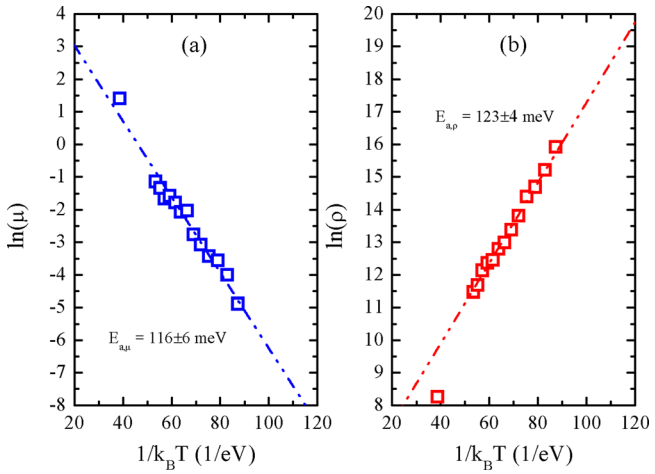

FIG. 7. (Color online) Temperature (range: 133–300 K) dependent Arrhenius plots (i.e., logarithmic of mobility or resistivity vs $1/k_BT$) for mobility (a) and resistivity (b) are used to determine the respective activation energies.

mobility data) and $E_{a,\rho} = 123 \pm 4$ meV (from resistivity data), respectively. The mobility and resistivity prefactors are $\mu_0 = 2.13 \times 10^2 \pm 1.46\,\mathrm{cm^2/V\,s}$ and $\rho_0 = 1.45 \times 10^3 \pm 1.32\,\Omega\,\mathrm{cm}$, respectively. The temperature dependent dark JV characteristics (data not shown) exhibit clamped current density measured at low temperatures and at relatively high forward biases. This is likely due to series resistance of the quasineutral region determined by the mobility of the majority carriers. Indeed, the activation energy of current density measured at 1.2 V is 114 meV, in good agreement with that of the mobility (116 meV).

While there are few reports in temperature dependent mobility in Cu(In,Ga)Se_2, there have been several reports on the temperature dependent conductivity in this material. Yan *et al.* reported the temperature dependent conductivity data (via Hall measurement) in one-stage RF sputtered deposited CIGS and reported two different slopes in the resistivity.[28] In the high- temperature regime (>120 K) the dominant transport mechanism is indicated as the thermionic emission transport with activation energy (increases with substrate temperature) of 90.6 meV which corresponds to samples grown at substrate temperature of 380 °C. Similar activation energy (98.1 meV) in the temperature dependent conductivity data was reported by Mesa *et al.* in which CIGS was deposited via three stage process.[4] In our case the substrate temperature is 435 °C and the observed activation energy in the resistivity plot ($= 123 \pm 4$ meV) is reasonable if substrate temperature plays an important role in the transport process.

The temperature dependent mobility or resistivity behavior in our study is similar to other cases of polycrystalline materials. Seto *et al.* demonstrated the theoretical model to describe the grain boundary (GB) scattering process and thermally activated mobility behavior in polycrystalline silicon films.[29] The charge transport in polycrystalline inorganic semiconductors has been extensively investigated before, in which the charge transport is limited by the presence of grain boundaries.[30,31] The activation energy, $E_{a,\mu}$, corresponds to the potential barrier height. The polycrystalline material comprises variable size crystallites separated by grain boundaries. The width of the grain boundaries is generally few atomic layers which are disordered structures and highly defective. The defect density in the grain boundary may vary and solely depend on the material growth process. More importantly, the grain boundaries become charged after trapping charge carrier and form potential barriers that impede carrier motion. This is why thermally activated Arrhenius-type charge transport is observed. The CIGS absorber in our solar cells is polycrystalline in nature and well characterized by the aforementioned transport mechanism. A pictorial representation of a vertical GB between two grains (Gs) in CIGS absorber (top) and the energy band diagram of CIGS absorber (bottom) in the presence of grain boundary[32–34] is shown in Fig. 8—which shows downward band bending with barrier height of φ_b.

The transport in polycrystalline materials depends on the grain size, grain boundary width, doping density in the grain, and defect density at grain boundaries. While the simple model of polycrystalline materials consisting of uniform distribution of grains and defect density (symmetric band profile across GB as in Fig. 8) has been used to explain the experimental observation, in reality we may have complicated distributions and structures. Because the potential fluctuation directly and adversely affects the key performance metrics of open-circuit voltage,[35] the reliable quantification of this quantity becomes increasingly important. Optical methods have been thus far the more often used methods, but they are sometimes hampered by issues such as requirement of fewer layers or incomplete devices, challenge of accessing the optical signals, spectral convolution due to graded bandgap, and so on. Rau *et al.* reviewed the research on the grain boundaries

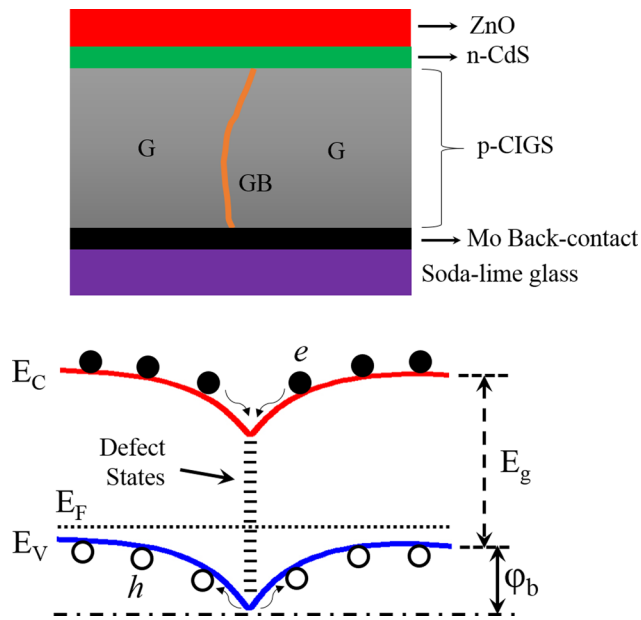

FIG. 8. (Color online) Top: Pictorial representation of CIGS device with grain (G) and a vertical GB in the CIGS absorber. Bottom: Energy band diagram in p-type CIGS absorber with downward band bending in the presence of a vertical GB. E_C, E_V, E_F, E_g, and φ_b are conduction band, valence band, Fermi level, bandgap, and the potential barrier height, respectively. The solid and empty circles represent the electrons and holes, respectively.

in polycrystalline Cu(In,Ga)(S,Se)$_2$ absorber alloy in thin-film solar cells and explained poor electronic activity of the grain boundaries in the charge transport.[36] According to the review of Rau *et al.*, the grain boundary potential is in the range of 100 to 300 meV and possesses dependency on Na content. Higher grain boundary potential is generally observed in Na free films. Note that the CIGS absorber used in this study was grown at a relative low temperature (435 °C) which may cause low Na diffusion from the soda lime glass and partially responsible for the low hole density in the absorber. Our estimated grain boundary potential barrier height (≈120 meV) is close to the $CuIn_{1-x}Ga_xSe_2$ device with x = 0.2% and 18% Cu content.[37] The evidence of potential fluctuation in CIGS solar cell was observed via temperature dependent photoluminescence spectroscopy with a reported value of 100 meV.[38] The Kelvin-probe force microscopy (KPFM) is a technique that measure the surface potential distribution and to estimate grain boundary barrier height.[39,40] There are several reports on the grain boundary barrier height measurements in the range of 150–200 meV in CIGS material using KPFM.[41–44] On the other hand, local electrical transport measurement using scanning probe microscopy technique in p-Cu(In,Ga)Se$_2$ shows the potential barrier height at grain boundary is 100 meV.[45] The major point in the reported values of the potential fluctuation in Cu(In,Ga)Se$_2$ is that the role of composition (Ga or Cu content and presence/absence of Na) is important. This study focuses on extracting the potential fluctuation (≈120 meV) from the charge transport properties in CIGS solar cells using admittance spectroscopy, thus demonstrates a simple electrical-only method applicable to complete solar cell device. However, a study of localized potential barrier height at grain boundary needs further examination via compositional study and kelvin probe force microscopy in this CIGS cell.

V. CONCLUSIONS

We use a classic and straightforward method based on coordinated capacitance–voltage techniques and bias dependent admittance spectroscopy to measure the resistivity, hole mobility, and their temperature dependency in the doped CIGS solar cell. In the temperature range of 133–300 K, the resistivity and mobility vary between 8.21×10^6–3.83×10^3 Ω cm and 7.55×10^{-3}–4.08 cm^2/V s, respectively. The temperature dependent mobility and resistivity shows thermally activated behavior with activation energy ≈120 meV, which is speculated to be directly tied to the potential fluctuation due to grain boundaries. This potential fluctuation agrees well with the values estimated by using optical and microscopy technique. This method and the observed results in the charge transport are useful for further optimization of material processing and device fabrication.

ACKNOWLEDGMENTS

This work was supported by the U.S. Department of Energy through Sunshot PVRD Grant No. DE-EE-0007541 "Crosscutting recombination metrology for expediting V_{OC} engineering."

[1]P. Jackson, R. Wuerz, D. Hariskos, E. Lotter, W. Witte, and M. Powalla, Phys. Status Solidi RRL **10**, 583 (2016).
[2]K. Kim, H. Park, G. M. Hanket, W. K. Kim, and W. N. Shafarman, Prog. Photovoltaics Res. Appl. **23**, 765 (2015).
[3]U. Rau and M. Schmidt, Thin Solid Films **387**, 141 (2001).
[4]F. Mesa, C. Calderón, and G. Gordillo, Thin Solid Films **518**, 1764 (2010).
[5]H. Wang, Y. Zhang, X. L. Kou, Y. A. Cai, W. Liu, T. Yu, J. B. Pang, C. J. Li, and Y. Sun, Semicond. Sci. Technol. **25**, 55007 (2010).
[6]T. Umehara, S. Iinuma, A. Sadono1, Y. Kurokawa, and A. Yamada, Jpn. J. Appl. Phys. **54**, 018001 (2015).
[7]A. Amara, A. Ferdi, A. Drici, J. C. Bernède, M. Morsli, and M. Guerioune, Catal. Today **113**, 251 (2006).
[8]A. Kokil, K. Yang, and J. Kumar, J. Polym. Sci., Part B **50**, 1130 (2012).
[9]S. Paul, B. Ellman, S. Tripathi, G. Singh, and R. J. Twieg, J. Appl. Phys. **119**, 145501 (2016).
[10]N. J. Dawson, M. S. Patrick, S. Paul, B. Ellman, A. Semyonov, R. J. Twieg, R. Matthews, E. Pentzer, and K. D. Singer, J. Appl. Phys. **118**, 85502 (2015).
[11]S. Paul, B. Ellman, S. Tripathi, and R. J. Twieg, J. Appl. Phys. **118**, 135702 (2015).
[12]N. J. Dawson, M. S. Patrick, K. Peters, S. Paul, B. Ellman, R. Matthews, E. Pentzer, R. J. Twieg, and K. D. Singer, Proc. SPIE **9616**, 96160B (2015).
[13]S. Paul, *Charge Transport in Liquid Crystalline Smectic and Discotic Organic Semiconductors: New Results and Experimental Methodologies* (Kent State University, Kent, OH, 2016), available at http://rave.ohiolink.edu/etdc/view?acc_num=kent1469836810.
[14]K. K. Tsung and S. K. So, J. Appl. Phys. **106**, 83710 (2009).
[15]Q. Long, S. A. Dinca, E. A. Schiff, M. Yu, and J. Theil, Appl. Phys. Lett. **105**, 42106 (2014).
[16]P. C. Africa, C. De Falco, F. Maddalena, M. Caironi, and D. Natali, Sci. Rep. **7**, 3803 (2017).
[17]K. Alberi, B. Fluegel, H. Moutinho, R. G. Dhere, J. V. Li, and A. Mascarenhas, Nat. Commun. **4**, 2699 (2013).
[18]S. W. Tsang, S. K. So, and J. B. Xu, J. Appl. Phys. **99**, 13706 (2006).
[19]N. D. Nguyen, M. Schmeits, and H. P. Loebl, Phys. Rev. B **75**, 075307 (2007).
[20]J. V. Li, A. M. Nardes, Z. Liang, S. E. Shaheen, B. A. Gregg, and D. H. Levi, Org. Electron. **12**, 1879 (2011).
[21]J. Lee, J. D. Cohen, and W. N. Shafarman, Thin Solid Films **480–481**, 336 (2005).
[22]Y. Wang, Q. Liang, J. Huang, D. Ma, and Y. Jiao, RSC Adv. **7**, 28494 (2017).
[23]Y. Xiao, H. Wang, S. Zhou, K. Yan, Z. Guan, S.-W. Tsang, and J. Xu, ACS Appl. Mater. Interfaces **7**, 13415 (2015).
[24]J. V. Li, X. Li, D. S. Albin, and D. H. Levi, Sol. Energy Mater. Sol. Cells **94**, 2073 (2010).
[25]S. A. Dinca, *Hole Drift Mobility Measurements in Polycrystalline Copper Indium Gallium Selenide* (Syracuse University, 2010), available at https://search.proquest.com/docview/877982497?pq-origsite=gscholar.
[26]S. A. Dinca, E. A. Schiff, W. N. Shafarman, B. Egaas, R. Noufi, and D. L. Young, Appl. Phys. Lett **100**, 103901 (2012).
[27]S. A. Dinca, E. A. Schiff, B. Egaas, R. Noufi, D. L. Young, and W. N. Shafarman, Phys. Rev. B **80**, 235201 (2009).
[28]Y. Yan, S. Li, Y. Ou, Y. Ji, C. Yan, L. Liu, Z. Yu, and Y. Zhao, J. Mod. Transp. **22**, 37 (2014).
[29]J. Y. W. Seto, J. Appl. Phys. **46**, 5247 (1975).
[30]S. Siebentritt, Thin Solid Films **480–481**, 312 (2005).
[31]J. W. Orton and M. J. Powell, Rep. Prog. Phys. **43**, 1263 (1980).
[32]K. Taretto and U. Rau, J. Appl. Phys. **103**, 94523 (2008).
[33]C. P. Muzzillo, Sol. Energy Mater. Sol. Cells **172**, 18 (2017).
[34]M. Gloeckler, J. R. Sites, and W. K. Metzger, J. Appl. Phys. **98**, 113704 (2005).
[35]U. Rau and J. H. Werner, Appl. Phys. Lett. **84**, 3735 (2004).
[36]U. Rau, K. Taretto, and S. Siebentritt, Appl. Phys. A **96**, 221 (2009).
[37]A. Virtuani, E. Lotter, M. Powalla, U. Rau, J. H. Werner, and M. Acciarri, J. Appl. Phys. **99**, 14906 (2006).
[38]S. A. Jensen, S. Glynn, A. Kanevce, P. Dippo, J. V. Li, D. H. Levi, and D. Kuciauskas, J. Appl. Phys. **120**, 63106 (2016).
[39]T. Ishii, T. Minemoto, and T. Takahashi, in *2014 IEEE 40th Photovoltaics Special Conference* (IEEE, 2014), pp. 3682–3684.
[40]M. Nonnenmacher, M. P. O'Boyle, and H. K. Wickramasinghe, Appl. Phys. Lett. **58**, 2921 (1991).

[41]C.-S. Jiang, R. Noufi, J. A. Abushama, K. Ramanathan, H. R. Moutinho, J. Pankow, and M. M. Al-Jassim, Appl. Phys. Lett **84**, 3477 (2004).
[42]C.-S. Jiang, R. Noufi, K. Ramanathan, J. A. AbuShama, H. R. Moutinho, and M. M. Al-Jassim, Appl. Phys. Lett. **85**, 2625 (2004).
[43]Y. Yan, C.-S. Jiang, R. Noufi, S.-H. Wei, H. R. Moutinho, and M. M. Al-Jassim, Phys. Rev. Lett. **99**, 235504 (2007).
[44]J. B. Li, V. Chawla, and B. M. Clemens, Adv. Mater. **24**, 720 (2012).
[45]D. Azulay, O. Millo, I. Balberg, H.-W. Schock, I. Visoly-Fisher, and D. Cahen, Sol. Energy Mater. Sol. Cells **91**, 85 (2007).